A&A 533, A118 (2011)
DOI: 10.1051/0004-6361/201014891

Astronomy & Astrophysics

STIS optical spectroscopy of the lobes of CRL 618

A. Riera[1,2,3], A. C. Raga[4], P. F. Velázquez[4], S. A. R. Haro-Corzo[4], and P. Kajdic[5]

[1] Departament de Física i Enginyeria Nuclear, Escola Universitària d'Enginyeria Tècnica Industrial de Barcelona, Universitat Politècnica de Catalunya, C. Comte Urgell 187, 08036 Barcelona, Spain
e-mail: angels.riera@upc.edu
[2] Departament d'Astronomia i Meteorologia, Universitat de Barcelona, Av. Diagonal 647, Barcelona, Spain
[3] Institut d'Estudis Espacials de Catalunya (IEEC-UPC), Spain
[4] Instituto de Ciencias Nucleares, Universidad Nacional Autónoma de México, Apartado Postal 70-543, CP 04510, México DF, Mexico
e-mail: [raga;pablo;haro]@nuclearesunam.mx
[5] Instituto de Geofísica, Universidad Nacional Autónoma de México, CP 04510, México DF, Mexico

Received 29 April 2010 / Accepted 22 July 2011

ABSTRACT

Context. Many proto-planetary nebulae show collimated structures sometimes showing multiple outflows.
Aims. We present the results of new optical spectroscopic observations (both medium (with a dispersion of 0.56 Å pixel^{-1}) and low (2.73 and 4.92 Å pixel^{-1} for the G430L and G750L gratings) spectral resolution) of the lobes of the proto-planetary nebula CRL 618 obtained with the Space Telescope Imaging Spectrograph on board of the *Hubble* Space Telescope.
Methods. We analyse the density structure and the excitation conditions of the lobes of CRL 618. The spectra obtained at medium spectral resolution (~50 km s^{-1}) allow us to quote the fraction of unscattered (intrinsic) Hα emission. We have also obtained dereddened emission line ratios of several features from the low spectral resolution spectra.
Results. We find that most of the analysed line ratios are reproduced by planar shocks moving through a dense medium (with pre-shock densities ~10^4 cm^{-3}) with shock velocities from 30 to 40 km s^{-1} (except the [O III]/Hβ line ratios which require shock velocities of 80 to 90 km s^{-1}). We find that the [S II]-weighted ionization fraction ranges from 0.015 to 0.06. The total densities derived from the electron density and the ionization fraction are ~10^5 to 10^6 cm^{-3}.
Conclusions. We conclude that the spectra of the lobes of CRL 618 can be margially reproduced by steady plane–parallel shock models for shock velocities which are significantly lower than the velocities at which the jet moves outwards (~200 km s^{-1}). These results are consistent with the predictions of a jet with a variable ejection velocity. The mirror-symmetry, the luminosity asymmetry between both lobes and the ejection velocity variability suggest that its central source may host a binary system.

Key words. ISM: jets and outflows – planetary nebulae: individual: CRL 618

1. Introduction

Discovered during the AFCRL infra-red survey (Walker & Price 1975), CRL 618 was first studied in detail by Westbrook et al. (1975), who identified it as an object in transition from the asymptotic giant branch (AGB) to a planetary nebula (PN), i.e. in the proto-planetary nebula phase (PPN). Since then CRL 618 has been the subject of numerous studies at different wavelengths.

Ground-based optical and near infra-red imaging of CRL 618 reveal two lobes of emission separated by a dark lane. The optical spectrum of CRL 618 is composed of a faint continuum and low-excitation emission lines. From early observations, the optical emission from the lobes has been known to have two components: emission lines arising within the lobes and reflected light (continuum and permitted emission lines) which originates near the star and is scattered by dust grains in the lobes (Schmidt & Cohen 1981 [SC81]; Trammell et al. 1993 [TDG93]). Several studies of the forbidden line spectra arising from the lobes have demonstrated that the emission is shock excited (TDG93; Sánchez Contreras et al. 2002 [SSG02]; Riera et al. 2006).

Surrounding the central star, there is a compact H II region elongated in the East-West direction, detected in the centimeter and millimeter-wave continuum (Kwok & Feldman 1981; Kwok & Bignell 1984; Martín-Pintado et al. 1988). The H II region is indirectly probed by scattered light: scattered Hα, Hβ, and high excitation lines are observed. It is characterized by high densities ($\geq 10^6$ cm^{-3}), higher than the critical densities of most forbidden lines (SC81).

The *Hubble* Space Telescope (HST) optical images of the shock-excited line emission have revealed spectacular collimated outflow structures (or jets) oriented in the East-West direction (Trammell & Goodrich 2002). These images reveal the mirror-(or reflexion) symmetry of the lobes of CRL 618. Several bow like features are seen within the lobes as well as two bright, bow-shaped structures at the tip of the lobes. The Hα HST image of CRL 618 also shows a bright compact nebulosity in the East lobe, labeled A′ by SSG02, which has a spectrum different from that of the lobes and similar to that of the central HII region. SSG02 suggested that region A′ is the outermost parts of the HII region surrounding the star. In addition to the Hα emission detected in the inner regions and the shocked lobes, a faint halo of emission is present in the Hα HST image (Trammell & Goodrich 2002), likely to be Hα emission scattered by dust present in the outer regions of CRL 618.

The jets mapped with the HST were known to have high velocities in optical lines (Carsenty & Solf 1982; SSG02). High

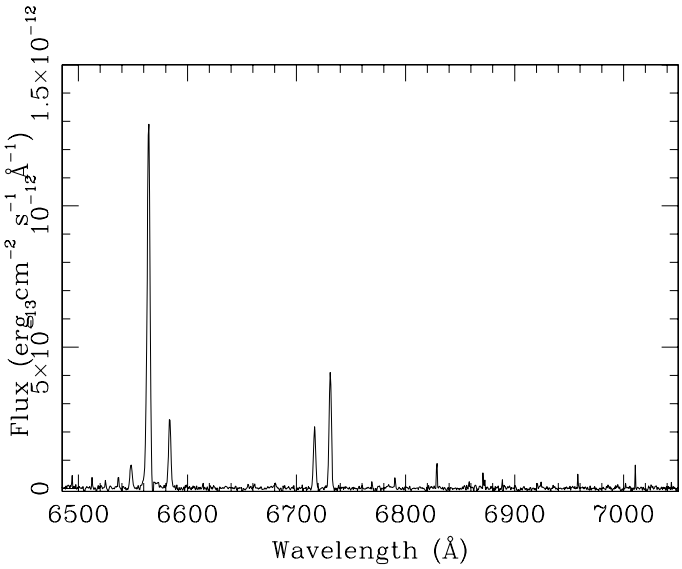

Fig. 1. Integrated spectrum of the bright lobe of CRL 618 obtained with the medium spectral resolution grating, where we observed the Hα, [N II] 6548, 6583 Å, and [S II] 6716, 6731 Å emission lines.

velocities and multiple outflows are also seen in molecular gas. Cox et al. (2003) detected high velocity features in H_2, associated with the optical jets (with velocities up to 200 km s^{-1}). Dense molecular gas (detected in CO) is also outflowing at velocities of the order of 200 km s^{-1} (e.g., Cernicharo et al. 1989; Neri et al. 1992).

In this paper we present the analysis of the excitation conditions of the lobes of CRL 618 based on archival STIS HST spectra. In Sect. 2 we describe the observations on which our analysis is based. In Sect. 3 we present the high spectral resolution observations and determine the fraction of the scattered Hα emission and describe the spatial distribution of the electron density. We present the analysis of the low spectral resolution spectra in Sect. 4, including the spatial distribution of several emission lines and a discussion of the excitation conditions in the lobes of CRL 618. Finally, we discuss our results in Sect. 5. The main conclusions of this work are summarized in Sect. 6.

2. Observations and reduction

We have analysed STIS data which were retrieved from the HST Data Archive[1]. The long slit spectra of the lobes of CRL 618 were obtained on 2003 December 20. They were originally part of Cycle 11 proposal 9430 (P.I: S. Trammell; see Sumerel & Trammell 2005). CRL 618 was observed using the 52″ × 0.″2 slit and the G430L, G750L and G750M gratings.

The G430L and G750L gratings were centered on λ_c = 4300 Å and 7751 Å, respectively. This configuration provides continuous wavelength coverage from 3000 to 10 250 Å. The instrumental parameters are summarized in Table 1. The observations through the low dispersion gratings (G430L and G750L) are used primarily to study the physical conditions and ionization structure of the lobes of CRL 618.

The observations obtained through the medium dispersion G750M grating centered on λ_c = 6768 Å, with a reciprocal dispersion of 0.56 Å pixel^{-1}, allow us to estimate the fraction of scattered Hα emission, and the spatial distribution of the density and the excitation conditions. The spectral range covered with the G750M grating includes Hα, [N II] 6548, 6583 Å and [S II] 6716, 6730 Å (see Fig. 1).

The 0.2″ width slit was oriented along the bipolar axis of CRL 618 (PA = 93°). Spectra were obtained at two positions with a spatial offset of 0.894″ perpendicular to the slit. The exposures were dithered 0.275″ along the slit to help to remove the hot pixels. However, the effect of the hot pixels affecting the [N II] 6583 Å emission line when using the G750M grating could not be removed. Therefore, we have only used the [N II] 6548 Å emission line for our analysis.

The long-slit STIS spectra were wavelength and flux calibrated at the Space Telescope Science Institute following the standard HST pipeline calibration and then shifted to create a single image at each position for the three gratings.

The two slit positions shown in Fig. 2 were determined by comparing the emission line distributions along the slit in the STIS spectra with the brightness cuts through the WFPC2 images of the nebula (with an accuracy of ±0.1″). Unfortunately, the slit positions are not ideal as the brightest regions were not included in the observations. In Fig. 2 we show the Hα archival HST image of CRL 618 (rotated so that the bipolar axis is approximately parallel to the ordinate) on which the two positions (called position 1 and position 2) of the slit of the STIS observations are shown.

Slit 1 slices through bright regions of both lobes, crossing a bow-shaped structure in the West lobe. In the bright East lobe the slit position 1 slices diffuse emission to the south of the bright compact nebulosity (see Fig. 2) and several bow-shaped, ripple-like features (Trammell & Goodrich 2002). Slit 2 crosses the East lobe, sampling several bow-shaped structures at the tips of the outflows. We have labeled many of the observed features from "a1" to "h1" for position 1, and from "a2" to "d2" for position 2, as shown in Fig. 2.

3. Medium dispersion spectroscopy

The Hα PV diagrams show the presence of two distinctly velocity components in the bright lobe, with one component stretching across the spectra at a radial velocity of ~40–50 km s^{-1} (hereafter the "RC" or red-shifted (scattered) component). In Fig. 3 we show the Hα, [S II] 6731 Å and [N II] 6548 Å PV diagrams obtained from the STIS position 2 spectra to illustrate the presence of the "RC" component.

In order to study the spatial distribution of both Hα components (i.e. the "RC" and the intrinsic components) in greater detail, the brightness surface distribution has been deduced for each Hα component using a single or a two components Gaussian line fit row by row (using the IRAF[2] package). This procedure has been applied to all spectra (obtained from slit positions "1" and "2"). We propose that the "blue" component of Hα observed in the bright lobe corresponds to the line emission arising from the lobe, and that the red-shifted component ("RC") correspond to emission originated in the central region

[1] Based on observations made with the NASA/ESA *Hubble* Space Telescope, and obtained from the *Hubble* Legacy Archive, which is a collaboration between the Space Telescope Science Institute (STScI/NASA), the Space Telescope European Coordinating Facility (ST-ECF/ESA) and the Canadian Astronomy Data Centre (CADC/NRC/CSA).

[2] IRAF is distributed by the National Optical Astronomy Observatories, which are operated by the Association of Universities for Research in Astronomy, Inc., under cooperative agreement with the National Science Foundation.

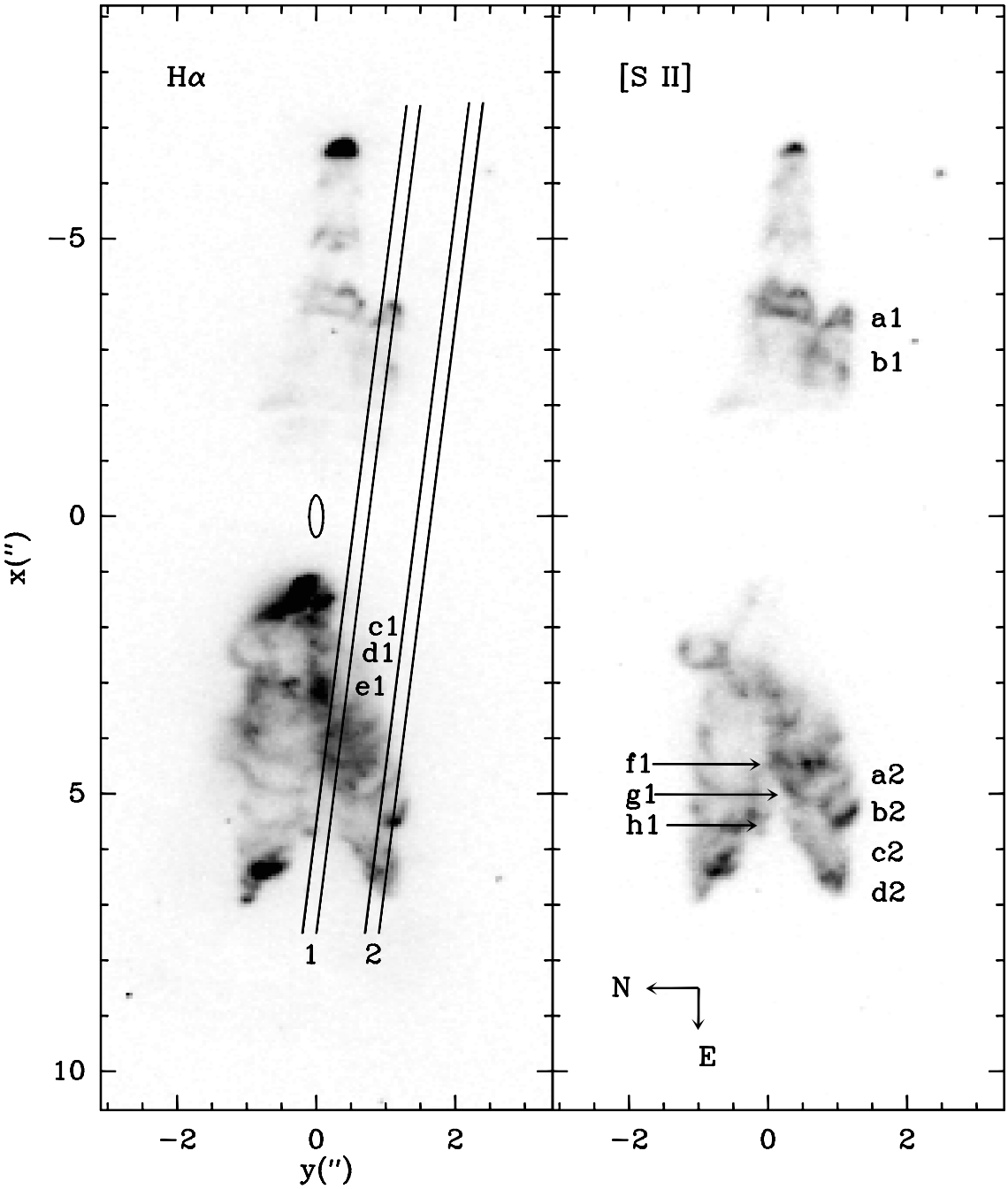

Fig. 2. *Left*: Hα archival HST image (with some contamination of [N II]) of CRL 618 shown with a linear scale (rotated so that the bipolar axis is approximately parallel to the ordinate). The STIS slit positions ("1" and "2") are superimposed to the HST image. The labels identify the position of several features. The compact central HII region (elongated in the East-West direction) is also overplotted to the Hα image. *Right*: [S II] archival HST image of CRL 618 shown with a linear scale (rotated so that the bipolar axis is approximately parallel to the ordinate). The labels identify the position of several features.

Table 1. STIS HST observations.

Slit position	Grating	Spectral Res. (Å/pixel)	λ_c (Å)	Exposure time (s)	Wavelength coverage (Å)	Data sets
Pos. 1	G750L	4.88	7751	1300	5260–10 250	o6ms06010,o6ms06020
Pos. 2	G750L	4.88	7751	650	5260–10 250	o6ms06030
Pos. 1	G430L	2.75	4300	1580	2900–5700	o6ms06060,o6ms06070
Pos. 2	G430L	2.75	4300	1600	2900–5700	o6ms06080,o6ms06090
Pos. 1	G750M	0.554	6768	825	6485–7050	o6ms060b0
Pos. 2	G750M	0.554	6768	1800	6485–7050	o6ms060c0, o6ms060d0

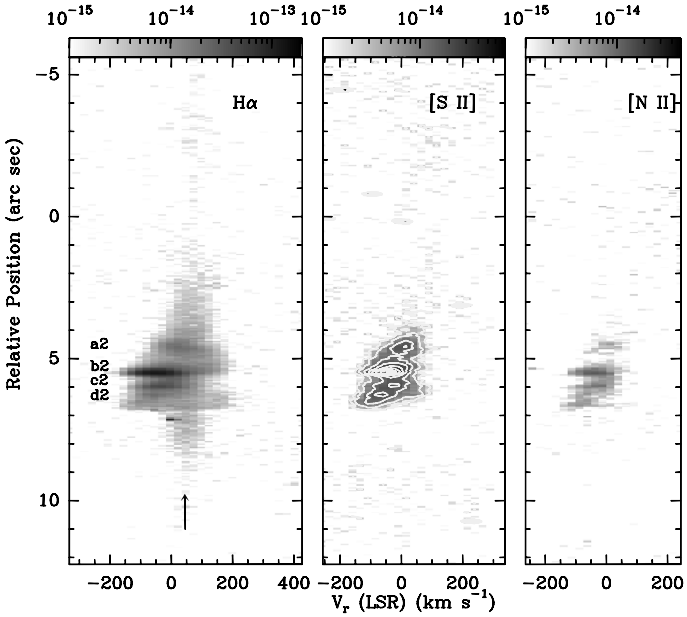

Fig. 3. Hα, [S II] 6731 Å and [N II] 6548 Å PV diagrams obtained from the STIS position 2 observations. The PV diagrams are shown with a logarithmic grey scales, with the fluxes given in units of erg cm^{-2} s^{-1} Å^{-1} arcsec^{-2} by the bars above each plot. Linear contours have been superposed to the [S II] PV map (white contours). The radial velocities were corrected by the systemic velocity (∼−21 km s^{-1}). The ordinate gives position along the slit. The zero position corresponds to the point along the slit closest to the central source. Spectral features are labeled. The vertical arrows aid to identify the redshifted component (see text).

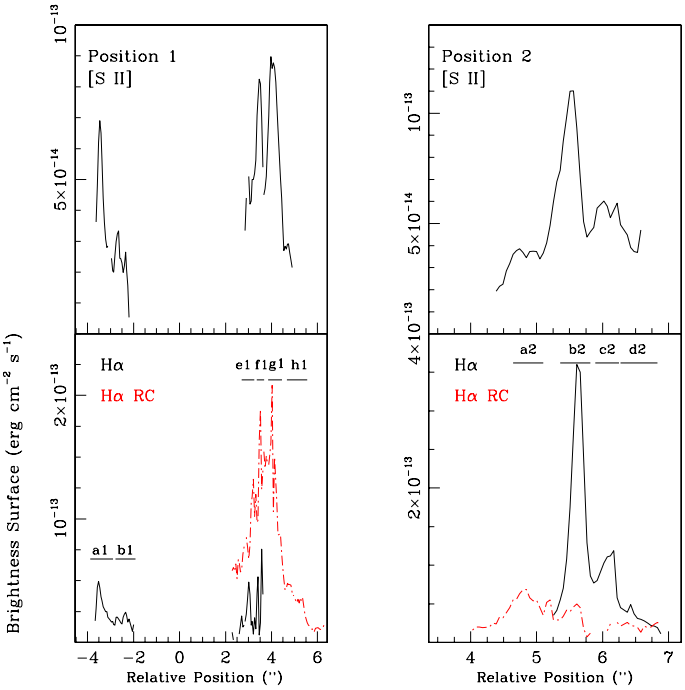

Fig. 4. Hα (*bottom panels*) and [S II] (6716+6731 (*top panels*) brightness profiles as a function of relative position for the spectrum obtained at position 1 (*left panels*) and slit position 2 (*right panels*). Solid lines correspond to intrinsic emission and the dot-dashed lines correspond to reflected emission (i.e., the "RC" component) (see text).

and scattered by dust grains in the lobes, as pointed out by Carsenty & Solf (1982). Carsenty & Solf found that their velocity data are compatible with an outflow of dust and gas which move nearly with the same velocity (∼80 km s^{-1}) with respect to the central region.

In the faint lobe, the "RC" and the unscattered emission can not be disentangled. Since the radial velocity of the Hα emission arising from "a1" and "b1" agrees well with that of the [S II] emission lines, we assume that the observed Hα emission arises from the lobe. Consequently, the Hα/[S II] and Hα/[N II] emission line ratios quoted in "a1" and "b1" are upper limits.

Figure 4 presents the distributions of the brightness surface of the both velocity components for the slit positions 1 and 2. We have quoted the fraction of the scattered Hα emission for "b2", "c2" and "d2" features, which are 15%, 12% and 41% respectively, in good agreement with the value of 17% determined spatially integrating along the bright lobe by TDG93.

3.1. Intrinsic emission: emission line ratios and nebular diagnostics

We have analyzed the line ratios (obtained from the single or two components Gaussian fit analysis) as a function of position along the slit. Figure 5 shows the spatial distribution of the [S II] 6716/6731, [S II](6716+6731)/Hα (=[S II]/Hα) and [N II] 3.88 × 6548/Hα (=[N II]/Hα) emission line ratios for slit positions 1 and 2. We have computed these emission line ratios from the unscattered (intrinsic) emission to evaluate the physical conditions of the outflowing gas.

The easiest emission line ratio to interpret is that of [S II] 6716/6731, which decreases monotonically with increasing electron density up to values of 10^4 cm^{-3}, i.e. the critical density of [S II]. In Fig. 5, we see large variations in the [S II] doublet ratio in the west lobe, where the lowest values are close to the high-density limit (i.e., [S II] doublet ratio ∼0.50 and electron densities ≥10^4 cm^{-3}). The relative errors of the [S II] line ratio range from 10% (at the brightest regions) to 30% at the faint ones.

In the bright East lobe observed along slit "1", the [S II] line ratio has an approximately position-independent value within the 0.50 to 0.60 range, corresponding to electron densities from 4000 to 10^4 cm^{-3}.

The [S II] 6716/6731 emission line ratio along the East lobe obtained for slit 2 (see Fig. 5) is mostly within the 0.45 to 0.70 range, corresponding to electron densities from 2000 to ≥10^4 cm^{-3}. If we draw a straight line in Fig. 5, passing through the peak of the [S II] ratio of features "a2" to "d2", we see that forms an upper envelope to all the values in this region. From this upper envelope, we deduce that the [S II] line ratio decreases (i.e. the electron density increases) from "a2" to "d2".

These values are in good agreement with previous ground based estimates although we have detected density structure at small scales which were not detected from the ground. The [S II] 6716/6731 line ratios determined in the spectroscopic studies of SC81, Kelly et al. (1992), TDG93, and Baessgen et al. (1997) give values of 0.55 ± 0.03 (0.52 ± 0.03) in the East (West) lobe. SSG02 evaluated the spatial distribution of the [S II] line ratio, obtained from ground-based spectroscopy, and found no systematic variations, with mean values of 0.55 and 0.50 for the East and West lobes, respectively.

Figure 5 shows the spatial distribution of the [S II]/Hα and [N II]/Hα ratios obtained from slit "1". Of particular interest is the high [S II]/Hα value observed along the faint West lobe, which shows a wide scatter with values mostly staying within a range of 1.0 → 1.8. In features "f1" and "g1", i.e. with intrinsic

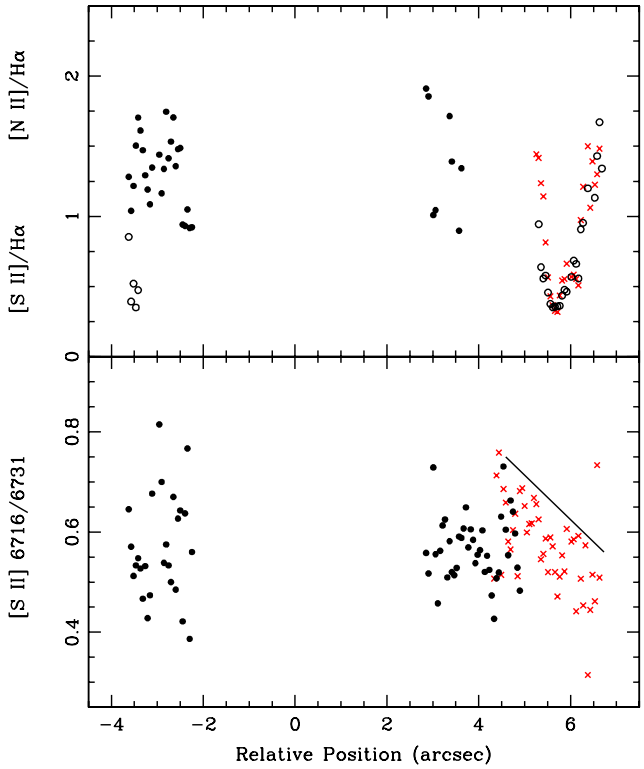

Fig. 5. [S II] 6716/6731 (*bottom*) and [S II] (6716 + 6731)/Hα and [N II] 6548/Hα ($\times$3.9) (*top*) obtained for the intrinsic emission as a function of relative distance. The filled dots correspond to points along slit position 1 and the red crosses correspond to points along slit position 2. The [N II] 6548/Hα ($\times$ 3.9) emission line ratios from the faint lobe (position 1) and from the "a2" to "d2" features (position 2) are also shown in the top panel (as open circles). We have drawn a stright line in the bottom panel passing through the peak of the [S II] ratio of features "a2" to "d2" to illustrate the decrease of the [S II] line ratio from "a2" to "d2".

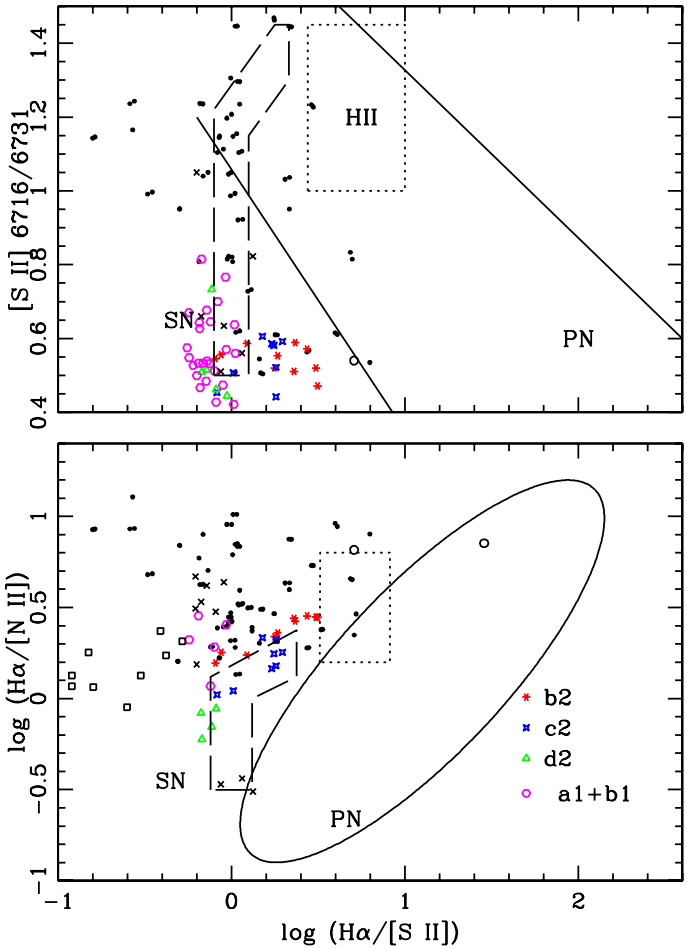

Fig. 6. Position of the CRL 618 features in the Hα/[S II] vs. Hα/[N II] and Hα/[S II] vs. [S II] 6716/6731 diagrams. In these diagrams the locations of the H II regions, SNRs and PNe are delineated by solid (PNe), long-dashed (SNRs) and dotted (HII regions) lines (adapted from Riesgo & López 2006). The HH objects (taken from the sample of Raga et al. 1996) are shown as black dots. We have also included several PPNe (taken from Raga et al. 2008) (crosses). The open squares correspond to the irradiated bow-shock models (Raga et al. 2008). The line ratios corresponding to the intrinsic emission of features "b2", "c2", "d2" and "a1+b1" are also plotted. The positions of "e1" and "d1" are also shown as open circles; these emission line ratios were obtained by summing across each feature.

Hα emission computed, the [S II]/Hα ratio also shows quite wide scatter, with values between 1.0 to 2.0.

Note the strong variability of the [S II]/Hα value within the bright lobe (slit "2"). In the region at relative distances from 5.5″ to 6.2″, i.e. from the [S II] emission peak of "b2" towards "c2", the [S II]/Hα ratio shows lower values than the ones reported from the spectra obtained at slit position 1, with values ranging from 0.25 to 0.70. At the edge of "b2" facing the source and at regions beyond "c2", the measured line ratio grows reaching a value of ∼1.5. The variations of the [N II]/Hα ratio follows the pattern of the [S II]/Hα ratio, suggesting that the strong variation is not due to excitation conditions but to an increase of the Hα flux.

In the following, we present a revised version of the diagnostic diagrams proposed by Sabbadin et al. (1977) to discriminate different classes of objects (HH objects, PNe, SNRs and HII regions) (Fig. 6). These diagrams also give information on the excitation mechanism (photoionization, shock excitation or mixed). In this figure we have adapted these diagrams including the most recent compilation of HH objects (Raga et al. 1996), a sample of proto-PNe (Raga et al. 2008) and the irradiated shock models from the work of Raga et al. (2008). The PN region is adopted from Riesgo & López (2006). We also plotted the points corresponding to different positions with a measure of the intrinsic Hα and [S II] doublet lines along the West and East lobes. The Hα/[N II] vs. Hα/[S II] diagram includes fewer data than the other because we obtained fewer measurements of the [N II] 6548 Å emission line. A detailed look at Fig. 6 reveals a large scatter in the log(Hα/[S II]) and log(Hα/[N II]) values (both within the range from −0.2 to 0.5).

As already mentioned, the features of CRL 618 show low values of the [S II] 6716/6731 ratio, similar to the lowest values shown by the sample of HH objects, which are indicative of large densities (up to $\gtrsim 10^4$ cm^{-3}).

The emission line ratios we obtained for CRL 618 cover regions of these diagnostic diagrams which are covered either by the HH objects and/or supernova remnants. This provides support to "pure" shock excitation as the mechanism responsible for the emission arising from the outflows. In the following, we analyze the excitation mechanism operating in "c1", "d1" and "e1". We note that the location of the "d1" feature in the log [N II]/Hα vs. log [S II]/Hα diagram (Fig. 6) confirms that photoionization is the dominant mechanism in "d1", confirming previous results. Feature "e1" falls close to the region outlined by the dense PN in the [S II] 6716/6731 vs. log [S II]/Hα diagram

Table 2. Observed line fluxes relative to [N I] 5200 Å. Position 1.

Emission line	a1	b1	d1	e1	f1	g1	h1
Hβ	0.33	–	–	2.16	1.20	1.16	–
[N I] 5200	1.	1.	–	1.	1.	1.	1.
[O III] 5007	–	–	–	–	0.30	0.15	–
I([N I])[a]	3.78	5.36	–	4.21	12.2	19.5	–

Notes. [(a)] [N I] 5200 unreddened intensity in units of 10^{-13} erg cm^{-2} s^{-1} arcsec^{-2}.

(see Fig. 6). This feature falls between the "d1" feature and the other features in the log [N II]/Hα vs. log [S II]/Hα diagram. To elucidate the nature of the "e1" feature we have computed the reddening-corrected [O I] 6300/Hα and [N I] 5200/Hβ line ratios (which also help to discriminate a photoionized spectrum from a shock-excited one). The values of the ratios of "e1" are in both cases between the values reported for "d1" and the mean value of the rest of features (observed along slit 1). The de-reddened [O I] 6300/Hα ratio is of ≈0.10 in "d1", 0.16 in "e1" and a mean value of 0.90 is measured at larger distances from the central source. The [N I] 5200 Å emission line was not detected at "d1". The de-reddened [N I] 5200/Hβ ratio has a value of 0.6 in "e1" and has larger values for the features at larger distances from the central source (see above). Hence, the spectrum of feature "e1" shows significant differences with respect to the other features. From this analysis, we conclude that the features located close to the central source ("c1", "d1" and "e1") have a spectrum which is dominated by a photoionized (reflected) component.

4. Low dispersion spectroscopy

One-dimensional spectra of each of the identified features were obtained by adding over the spatial extent of each feature. For each of these spectra, we measured line fluxes by fitting Gaussian to the observed line profiles. At the spectral resolution of 4.92 Å provided by the G750L grating the scattered and intrinsic Hα emission cannot be measured separately, and [N II] 6548, 6583 Å and the Hα 6563 Å emission lines are significantly blended. Despite this caveat the fitting of triple profiles using Gaussians is an acceptable procedure since restrictions can be applied to the fit. We fixed the [N II] 6583/6548 flux ratio to 2.88 and the relative line positions of the three lines [N II] 6548, 6583 Å and Hα. The deblending procedure adds uncertainty to the [N II] 6583 and Hα fluxes, which in our estimate does not exceed 20%. We do not attempt to deblend the [S II] 6716 and 6731 Å emission lines. The resulting emission line density fluxes are listed in Tables 2, 3 and 4, 5 for slit positions 1 and 2, respectively.

4.1. Emission line fluxes and surface brightness profiles

The observed spectra are characterized by the presence of low ionization forbidden lines ([O I], [N I], [S II], [C I]), intermediate ionization lines ([O II], [N II], [S III]), and a hint of [O III], and HI Balmer lines. These lines were already detected and identified in previous ground-based spectroscopic observations of this object (e.g., Kelly et al. 1992).

Figure 7 shows the spatial distribution of the relative surface brightness of bright emission lines for position 1. This figure only shows the relative emission distributions (all of the emission line distributions are normalized to their peak values).

Table 3. Observed line fluxes relative to [O I] 6300 Å. Position 1.

Emission line	a1	b1	d1	e1	f1	g1	h1
[O I] 6300	1.	1.	1.	1.	1.	1.	1.
Hα	1.25	0.95	11.0	6.90	2.45	2.64	2.95
[N II] 6583	0.32	0.12	1.10	0.75	0.32	0.29	0.40
[S II] 6725	1.14	1.12	0.46	1.37	0.87	0.92	1.15
[C aII] 7290	0.10	–	–	–	–	–	–
[O II] 7325	0.21	0.17	2.90	1.42	0.35	0.35	0.47
[S III] 9533	–	–	3.76	0.96	–	0.20	–
[C I] 9825+9850	0.64	1.45	–	2.57	1.36	0.67	–
I([O I])[a]	1.53	2.70	0.46	1.23	5.80	7.57	2.05

Notes. [(a)] [O I] 6300 unreddened intensity in units of 10^{-12} erg cm^{-2} s^{-1} arcsec^{-2}.

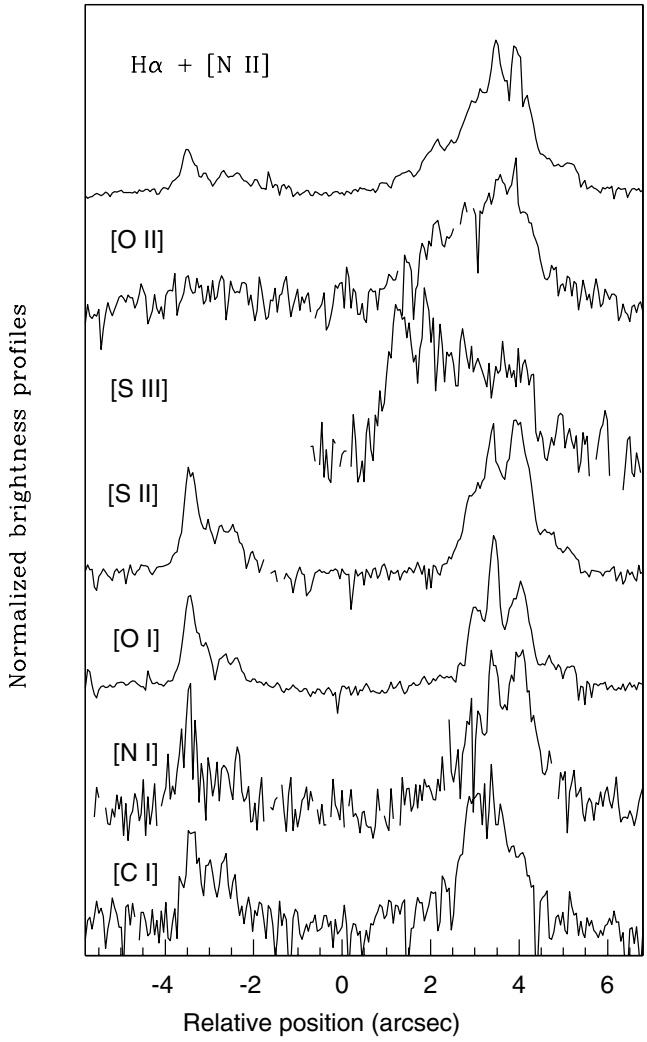

Fig. 7. Hα + [N II] 6548,6583, [O II] 7325, [S III] 9533, [S II] 6716+6731, [O I] 6300, [N I] 5200 and [C I] 9825+9850 surface brightness profiles (integrated over all the radial velocity range in which line emission is detected) as a function of relative position for the spectrum obtained at position 1.

Of particular interest is the spatial distribution of the intermediate excitation emission lines relative to the low ionization ones (see Fig. 7). Spatial brightness distributions from low ionization species, such as NI, OI and SII, are generally similar to one another, but are considerably different from the lines of higher ionization. Features beyond "e1" (i.e. at larger distance from the

Table 4. Observed line fluxes relative to [N I] 5200 Å. Position 2.

Emission line	a2	b2	c2	d2
Hβ	0.71	1.25	1.11	0.80
[N I] 5200	1.	1.	1.	1.
[O III] 5007	–	0.32	0.17	–
I([N I])[a]	1.05	1.83	1.50	1.18

Notes. [a] [N I] 5200 unreddened intensity in units of 10^{-12} erg cm^{-2} s^{-1} arcsec^{-2} .

Table 5. Observed line fluxes relative to [O I] 6300 Å. Position 2.

Emission line	a2	b2	c2	d2
[O I] 6300	1.	1.	1.	1.
Hα	1.92	1.58	1.36	2.20
[N II] 6583	0.57	0.45	0.65	0.43
[S II] 6725	1.21	0.69	0.67	0.91
[Ca II] 7290	–	–	0.10	–
[O II] 7325	0.18	0.26	0.21	–
[S III] 9533	–	–	–	–
[C I] 9825+9850	0.86	0.23	–	–
I([O I])[a]	2.85	12.0	8.10	4.08

Notes. [a] [O I] 6300 unreddened intensity in units of 10^{-12} erg cm^{-2} s^{-1} arcsec^{-2}.

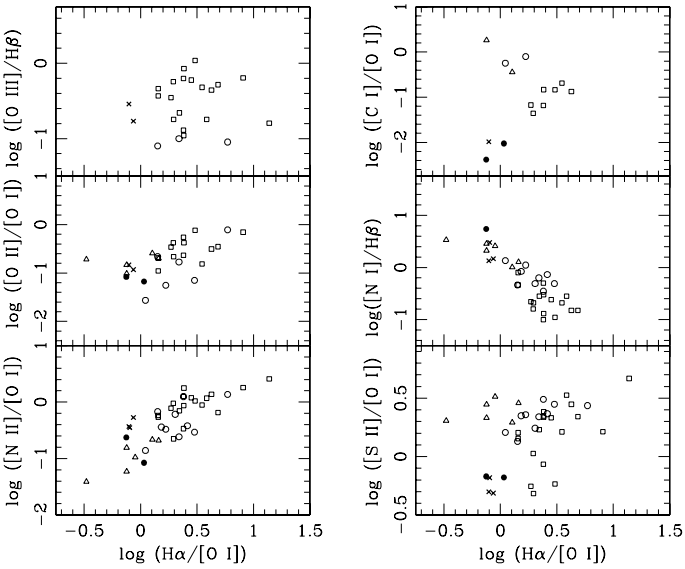

Fig. 8. Graph showing six emission line ratios as a function of Hα/[O I] 6300 for several regions of CRL 618 and HH objects (from the compilation of Raga, Böhm & Cantó 1996). Filled circles correspond to features "a1" and "b1" (faint lobe) and crosses correspond to "b2", "c2" and "d2". The points corresponding to HH objects are shown with open symbols: the high excitation spectra are shown as open squares, the intermediate excitation spectra are the open circles and the low excitation spectra are the open triangles.

central source) are very prominent in low ionization species. The innermost regions of the East lobe (features "c1" and "d1") have weak counterparts in low ionization species. [S III] is limited in extent to the innermost regions of the East lobe, showing its intensity peak at "c1". The Hα + [N II] and [O II] lines are intermediate in distribution between [S III] and low ionization lines, since emission is detected at all positions along the East lobe. The Hα + [N II], [O II] and low-ionization lines (except [C I] 9825, 9850 Å) peak at the same spatial positions. Features "a1" and "b1" (in the faint lobe) are conspicuous in all low ionization lines. Such spectral properties confirm the idea that different excitation mechanism is responsible for the spectra observed at "c1", "d1" and "e1" than at the rest of the features.

4.2. Emission line ratios and excitation conditions

Tables 2–5 list the line intensities obtained from the low dispersion spectroscopic observations (as described below). In order to obtain emission line ratios that represent the unscattered emission (i.e., the emission locally produced within the lobes), we have corrected the observed Hα and Hβ emission line intensities using the fraction of scattered Hα emission computed in this work (see Sect. 3.1) and assuming a non-selective scattering. We also assume that all forbidden emission lines are produced within the lobes. The former assumption is supported by the results of SC81 and TDG93.

From the unscattered line intensities we have obtained a set of line ratios which have been de-reddened employing the mean interstellar curve of Savage & Mathis (1979) and an $E(B-V)$ values of 1.3 (East lobe), and 2.1 (West lobe) (TDG93). The uncertainty of the line ratios including Hα depends on the uncertainty of the Gaussian fit applied to separate the scattered and intrinsic emission, which is $\lesssim$10% at the bright regions. Moreover, the necessity of deblending Hα from [N II] 6548, 6583 Å causes estimated error of ratios involving Hα or [N II] emission lines to be $\lesssim$20%. For the rest of ratios, the errors come from the uncertainty in the determination of the extinction and the assumption that all the forbidden emission lines arise from the lobes.

In the following we analyze the emission line ratios of the shock-excited regions (a1, b1, b2, c2,d2). The [S II]/[O I] ratio is primarily sensitive to density. As the critical density of [O I] 6300 Å ($\sim 10^6$ cm^{-3}) is significantly larger than the critical density of [S II] 6716, 6731 Å ($\sim 10^4$ cm^{-3}), the [O I] 6300 Å line becomes stronger relative to [S II] (6716+ 6731) Å as the density increases. The lowest [S II]/[O I] values are found in the East lobe.

The [N II] 6583/[O I] 6300 ratio depends primarily on the ionization fraction. This ratio shows a a significant scatter (with values in the range from 0.1 to 0.6) along the shock-excited features (the highest values are found in the structures observed at slit position 2). The [N I]/Hβ ratios show values $\sim$0.7 $\rightarrow$ 3. The [O III] 5007 Å emission lines are only detected in the East lobe. The [O III] 5007/Hβ show values of 0.3 and 0.2 in "b2", "c2", respectively.

In Fig. 8 we plot the values observed in several features of the lobes of CRL 618 together with a sample of spectra of HH objects taken from the compilation of Raga et al. (1996). Raga et al. classified the HH spectra as "high excitation", "intermediate excitation" and "low excitation" according to their [O III] 5007/Hβ and [S II] (6716+6731)/Hα ratios. To compare the spectra of CRL 618 with the sample of HH objects we have to consider that CRL 618 is likely to be a type I PN (TDG93; Riera et al. 2006). TDG93 derived log N/O = 0.0 ± 0.3 (East lobe) and 0.4 ± 0.4 (West lobe), which imply that CRL 618 is N-enriched with a N-abundance value compatible with the mean value of type I PNe (Kingsburgh & Barlow 1994).

To interpret the [N II]/[O I] versus Hα/[O I] and [N I]/Hβ versus Hα/[O I] diagnostic plots we have to keep in mind that the N/H abundance ratio of the CRL 618 is few times ($\lesssim$5) that of the HH objects In the [N II]/[O I] versus Hα/[O I] plot, CRL 618 partially overlaps the region where the low-excitation

HH objects lie. The [N I]/Hβ ratios for CRL 618 are difficult to interpret since this ratio is also collisionally de-excited at the large densities of CRL 618. The "scaled" [N I]/Hβ ratios for CRL 618 would then lie in the region of low-to-intermediate excitation HH objects. The [S II]/[O I] vs. Hα/[O I] diagnostic plot shows that most of the HH objects lie in a region with log ([S II]/[O I]) ~0.1 to 0.6, with a few high excitation HH objects showing log ([S II]/[O I]) < 0.0. The points of CRL 618 all lie in the former region, which correspond to HH objects with densities larger than the critical densities of [S II] 6716, 6731 Å.

Where [O III] emission is detected, the de-reddened [O III]/Hβ ratios show values just above the value defining the "high excitation" group (i.e. [O III]/H$\beta \geq 0.1$).

5. Interpretation

We try to determine the shock velocities that best explain the emission line ratios observed in the lobes of CRL 618. We have compared the de-reddened emission line ratios ([N I]/Hβ, Hα/[O I], [N II]/[O I] and [S II]/Hα) of "a1", "b1", "f1", "b2","c2" and "d2" with the grid of planar shock models of Hartigan et al. (1994) (for the $n = 10^4$ cm^{-3} preshock density), which cover a velocity range from 15 to 90 km s^{-1}. For most features, all the analyzed emission line ratios of low ionization lines (i.e. [N I]/Hβ, [S II]/Hα and [O I]/Hα) are reproduced by plane-parallel stationary shock models with velocities from 30 to 40 km s^{-1}. We should point out that there is a partial ambiguity in the Hα/[O I] velocity determination. The models with $V_s = 30$ to 40 km s^{-1} and with $V_s = 120$ to 140 km s^{-1} have line ratios similar to each other (Hartigan et al. 1987)), and to the ones observed in CRL 618. We have chosen a fit with the lower shock velocity models which agrees with the shock velocities obtained from the other emission line ratios (with the exception of [O III]/Hβ). Finally, [O III] emission was detected in "f1", "b2" and "c2". The observed [O III]/Hβ line ratios require shock velocities of the order of 80 to 90 km s^{-1}.

Hartigan et al. (1994) also computed a [S II]-weighted ionization fraction ($\langle I \rangle$) (defined in their Eq. (1)) which allows to convert the electron density measured from the [S II] line ratio to a total density. From the [S II] 6716/6731 and Hα/[S II] line ratios presented in Fig. 6, we have obtained the $\langle I \rangle$ values corresponding the various features. The values measured at "a1", "b1" and "d2" features imply $\langle I \rangle$ values from 0.015 to 0.020, which, together with the observed electron densities result on total densities of $\sim 3 \times 10^5$ cm^{-3}. Larger $\langle I \rangle$ values have been derived for "b2" and "c2" features, with values within the range from 0.03 to 0.06. The total densities derived for these features range from 10^5 to 10^6 cm^{-3}.

6. Summary and conclusions

Using STIS spectra (obtained from the HST archive) of the lobes of CRL 618, we have obtained medium- and low-resolution spectra (with a continuous wavelength coverage from 3000 to 10 250 Å) of several features of the lobes.

All analyzed features (with the exception of "c1", "d1" and "e1") are shock-excited. We have carried out a comparison of the shock excited regions with a sample of spectra of HH objects (from Raga et al. 1996). In the two-line ratio diagnostic diagrams, we see that the spectra of the jets of CRL 618 are compatible with the spectra of HH objects with an intermediate excitation. Shock velocities for CRL 618 calculated from our line ratios lie in a narrow range between 30 and 40 km s^{-1}, except for the [O III]/Hβ line ratios which require larger shock velocities (~80–90 km s^{-1}). The predicted shock velocities are significantly lower than the velocities at which the jet moves outwards (deprojected expansion velocities range from ~200 km s^{-1} (SSG02) up to 500 km s^{-1} (obtained by Balick et al. 2011, from proper motion measurements). The total densities derived for these features range from 10^5 to 10^6 cm^{-3}.

The HST images of CRL 618 have revealed the mirror-symmetry of the lobes of CRL 618. This kind of symmetry is also observed in other PPNe and young PNe (Sahai 2000). We should also note the brightness asymmetry between the West and East lobe. SSG02 quoted the dereddened luminosity of the [O I] emission line of the both lobes. They found that the dereddened [O I] luminosity of the west lobe is ≈75% that of the bright lobe.

The morphology and spectral properties of CRL 618 as seen by the HST, are reminiscent of HH jets. The observed structure within HH jets is often attributed to periodic or pulsed variations of the ejection velocity. The existence of a time dependent collimated outflow or jet acting during the PPN transition phase has been studied over the last 10 years. Periodic variations of the ejection velocity have been recently invoked to reproduce the morphology and kinematics of the PPNe Hen 3-1475 (Velázquez et al. 2004), and CRL 618 (Lee 2009) and the outer bow-shocks of the point-symmetric PN IC 4634 (Guerrero et al. 2008). Planetary nebulae simulations have also been carried forward which include the efects of clumps (Steffen & López 2004).

The multipolar morphology of CRL 618 led Dennis et al. (2008) to favour the "clumps" model over jets for this object. In the "clumps" model the multipolar geometry appears as a result of clumps outflowing along different directions. These clumps could arise from an explosive driven polar shell (Matt et al. 2006). The "clumps" model proposed by Dennis et al. (2008) could explain the multipolar morphology and the ramps of increasing radial velocity with distance to the flow origin. It is not clear, however, how the "clumps model" can reproduce the observed excitation conditions. Recently, Yirak et al. (2009, 2011) proposed the "clumped" jet model to reproduce the overall morphology of the HH jets. They assume the presence of clumps within the jet beam with random locations, sizes and velocities. The "clumped" jet model predicts nonaxial, co-moving bow-shocks which could reproduce the multipolar appearance of CRL 618.

Alternatively, the mirror-symmetry (or multipolar geometry) may be caused by the orbital motion of a binary system (i.e., the jet source is moving in an orbit around a stellar companion) (Haro-Corzo et al. 2009; Raga et al. 2009). Haro-Corzo et al. (2009) computed three-dimensional hydrodynamical simulations of a jet launched from the secondary star of a binary system. The primary star is the source of the AGB wind, and the two stars have a close eccentric orbit. The predicted maps for certain values of the input parameters exhibit either point-symmetric or mirror-symmetric substructures depending on the orientation of the flow with respect to the observer. Also, the maps exhibit different luminosities for the two lobes in the runs with a tilt between the jet axis and the orbital axis. The predicted asymmetries in the [N II] emission line is compatible with the value quoted for CRL 618 (as described above).

The presence of a high velocity molecular emission is also found in several HH jets, and it is explained either as ambient gas shocked and dragged along with the jet throught steady entrainment or it is asummed that the jet is molecular (i.e. intrinsically molecular or entraining core material). The first scenario should be ruled out as responsible for the high velocity molecular outflow in CRL 618 due to the high density values derived from the optical lines (Suttner et al. 1997). The presence of a molecular

jet in CRL 618 was proposed by Sánchez Contreras et al. (2004) and Lee et al. (2009). The presence of a molecular jet, which could not originate from the source of the HII region, reinforces the binary system scenario (with the jet source in orbital motion around a remnant AGB star) for CRL 618.

The mirror-symmetry and the luminosity asymmetry exhibit by both lobes of CRL 618 suggest that its central source may host a binary system. This point requires more numerical simulations of a binary system with an episodic jet suited to fit the observed properties of CRL 618.

Acknowledgements. We thank an anonymous referee for many helpful comments. The work of A.R. was supported by the MICINN grant AYA2008-06189-C03 and AYA2008-04211-C02-01 (co-funded with FEDER funds). A.C.R., P.F.V. and S.A.R.H.C. acknowledge support from UNAM grant, CONACyT grant 61547, and DGAPA-UNAM grants IN108207.

References

Baessgen, M., Hopfensitz, W., & Zweigle, J. Z. 1997, A&A, 325, 277
Balick, B., Gomez, T., Frank, A., et al. 2011, Asymmetric Planetary Nebulae V, ed. A. A. Zuijlstra, F. Lykou, I. Mc Donald, E. Lagadec, Jodrell Bank Centre for Astrophysics, Manchester, UK
Carsenty, U., & Solf, J. 1982, A&A, 106, 307
Cernicharo, J., Guelin, M., Martín-Pintado, J., Penalver, J., & Mauersberger, R. 1989, A&A, 222, L1
Cox, P., Huggins, P. J., Maillard, J.-P., et al. 2003, ApJ, 586, L87
Dennis, T. J., Cunningham, A. J., Frank, A., et al. 2008, ApJ, 679, 1327
Guerrero, M. A., Miranda, L. F., Riera, A., et al. 2008, ApJ, 683, 272
Hartigan, P., Raymond, J., & Hartmann, L. 1987, ApJ, 316, 323
Hartigan, P., Morse, J. A., & Raymond, J. 1994, ApJ, 436, 125
Haro-Corzo, S. A. R., Velázquez, P. F., Raga, A. C., Riera, A., & Kajdic, P. 2009, ApJ, 703, L18
Kelly, D. M., Latter, W. B., & Rieke, G. H. 1992, ApJ, 395, 174
Kingsburgh, R. L., & Barlow, M. J. 1994, MNRAS, 271, 257
Kwok, S., & Bignell, R. C. 1984, ApJ, 276, 544
Kwok, S., & Feldman, P. A. 1981, ApJ, 247, L67
Lee, C.-F., & Sahai, R. 2003, ApJ, 586, 319
Lee, C.-F., Hsu, M.-C., & Sahai, R. 2009, ApJ, 696, 1630
Martín-Pintado, J., Bujarrabal, V., Bachiller, R., Gómez-González, J., & Planesas, P. 1988, A&A, 197, L15
Matt, S., Frank, A., & Blackman, E. G. 2006, ApJ, 647, L45
Neri, R., García-Burillo, S., & Guelin, M. 1992, A&A, 262, 544
Raga, A. C., Böhm, K. H., & Cantó, J. 1996, Rev. Mex. Astron. Astrofis., 32, 161
Raga, A. C., Riera, A., Mellema, G., Esquivel, A., & Velázquez, P. F. 2008, A&A, 489, 1141
Raga, A. C., Esquivel, A., Velázquez, P. F., et al. 2009, ApJ, 707, L6
Riesgo, H., & López, J. A. 2006, Rev. Mex. Astron. Astrofis., 12, 174
Riera, A., García-Lario, P., Manchado, A., & Bobrowsky, M. 2001, Astrophys. Space Sci. Libr., 265, 209
Riera, A., Binette, L., & Raga, A. C. 2006, A&A, 455, 203
Sánchez Contreras, C., Sahai, R., & Gil de Paz, A. 2002, ApJ, 578, 269
Sánchez Contreras, C., Bujarrabal, V., Castro-Carrizo, A., Alcolea, J., & Sargent, A. 2004, ApJ, 617, 1142 (SSG02)
Sabbadin, F., Minello, S., & Bianchini, A. 1977, A&A, 60, 147
Sahai, R. 2000, ApJ, 537, L43
Savage, B. D., & Mathis, J. S. 1979, ARA&A, 17, 73
Schmidt, G. D., & Cohen, M. 1981, ApJ, 246, 444 (SC81)
Schwarz, H. E., Aspin, C., Corradi, R. L. M., & Reipurth, B. 1997, A&A, 319, 267
Steffen, W., & López, J. A. 1998, ApJ, 508, 696
Sumerel, A. N., & Trammell, S. R. 2005, BAAS, 37, 1161
Suttner, G., Smith, M. D., Yorke, H. W., & Zinnecker, H. 1997, A&A, 318, 595
Trammell, S. R., & Goodrich, R. W. 2002, ApJ, 579, 688
Trammell, S. R., Dinerstein, H. L., & Goodrich, R. W. 1993, ApJ, 402, 249 (TDG93)
Velázquez, P. F., Riera, A., & Raga, A. C. 2004, A&A, 419, 991
Volker, R., Smith, M. D., Suttner, G., & Yorke, H. W. 1999, A&A, 343, 953
Walker, R. G., & Price, S. D. 1975, AFCRL Technical Report 75-0373
Westbrook, W. E., Willner, S. P., Merrill, K. M., et al. 1975, ApJ, 202, 407
Yirak, K., Frank, A., Cunningham, A. J., & Mitran, S. 2009, ApJ, 695, 999
Yirak, K., Schroeder, E., Frank, A., & Cunningham, A. J. 2011, ApJ, submitted [arXiv:1101.6020]